ARCHIVES OF ELECTRICAL ENGINEERING VOL. 74(1), pp. 63–81 (2025)

DOI 10.24425/aee.2025.153013

# Efficient control of low inductance brushless DC motors based on LC filtering and active damping

**ALLAGUI MEHDI, ABBES MOHAMED**✉

*Laboratory LaTICE, Université de Tunis, ENSIT*
*Av Taha Hussein, Montfleury, 1008, Tunisia*
*e-mail:* ✉ *mohamed.abbes@esstt.rnu.tn, mahdi.alegui@enseignant.edunet.tn*

(Received: 06.07.2024, revised: 31.01.2025 )

**Abstract:** Brushless DC motors (BLDC) present several technical advantages with respect to conventional permanent magnets synchronous motors. These advantages include higher rotational speeds, reduced construction complexity and simpler control strategies. This paper discusses a cost-effective control strategy for BLDC motors characterized by low stator inductance. The proposed technique is based on an LC filter inserted between the inverter output and the motor. The filter capacitors are controlled such that three DC voltages are applied to the stator terminals. An active damping approach is used to control stator currents and prevents voltage oscillations. Compared with existing solutions, this technique simplifies the hardware implementation of such a drive system and offers a notable reduction in the switching frequency with minimal values of the magnetic elements. In addition, high frequency torque ripples are significantly reduced. The design procedure of this controller is presented in this paper and the performances are compared with the conventional control technique.

**Key words:** active damping, BLDC motor, low stator inductance, LC filter

## 1. Introduction

Brushless DC motors use permanent magnets to energize the rotor circuit. The rotating flux of the rotor generates trapezoidal back-EMFs through the stator phases. BLDC motors substantially reduce the audible noise and the electromagnetic interferences (EMIs) and offer a higher power to mass ratio compared with DC motors. For maximum torque operation, the control strategy should impose a DC current which flows through only two phase windings while the third phase is floating [1]. Phase commutations are achieved when the rotor travels 60 electrical degrees by energizing the phases that will produce the most amount of torque. In sensored control techniques, the rotor position is measured through Hall effect sensors. However, in order to

© 2025. The Author(s). This is an open-access article distributed under the terms of the Creative Commons Attribution-NonCommercial-NoDerivatives License (CC BY-NC-ND 4.0, https://creativecommons.org/licenses/by-nc-nd/4.0/), which permits use, distribution, and reproduction in any medium, provided that the Article is properly cited, the use is non-commercial, and no modifications or adaptations are made.

www.czasopisma.pan.pl PAN POLSKA AKADEMIA NAUK www.journals.pan.pl



simplify the hardware setup, sensorless control strategies were also adopted in many industrial applications [2]. Several varieties of general-purpose BLDC motors are available on the market with rated powers ranging from tens of Watt to few kW. Whatever the power range, most BLDC motors are characterized by low inductance values of stator windings, which results in high current ripples, and increased vibration of the drive system [3]. In order to attenuate current ripples, the most obvious solution was to increase the switching frequencies of power converters. This solution, although its simplicity, leads to higher switching losses and stringent electromagnetic requirements for the design of the six-switch inverter, particularly, in the medium and high power ranges. A more straightforward approach was used in [4] and consists in inserting series inductors between motor and inverter terminals. However, high inductance values prevent fast current switching during phase-to-phase commutations and, consequently, leads to a pulsating torque behaviour. Besides, the problems of congestion and inductor saturation impair the effectiveness of this solution. Therefore, the low inductance value represents an additional challenge for the design of competitive drive systems based on these actuating devices.

To avoid the aforementioned drawbacks, different advanced control schemes were analysed in literature. In references [5–7], it was shown that current ripples are effectively reduced if the DC link voltage is adapted according to the back-EMF induced in the stator phases. Thus, it was possible to suppress the torque ripple by inserting a buck-boost converter between the DC energy source and the two-level inverter. The buck converter with redundant switches has been also used in [8], to develop a fault-tolerant control of low inductance BLDC drives. In this same perspective, a 180° commutation logic was adopted in [9] for torque ripple reduction. Advanced PWM strategies are presented in [10] to deal with the issue of low inductance values. A deadbeat digital controller was developed in [11], allowing one to double the output equivalent frequency from 50 to 100 kHz.

Thus, recent research works have mainly used cascaded converter topologies and hysteresis controllers for effective control of BLDC motors with low stator inductance. These solutions lead to complex configurations of drive systems or increase the switching losses in power transistors. This paper proposes a simple and high-performance method for controlling low inductance BLDC motors. The proposed solution is based on an LC filter which offers a notable harmonic reduction and low-cost implementation. An active damping approach is used to control stator currents and prevents voltage oscillations. Although LC filtering has been used in [12, 13] for harmonic mitigation in BLDC drive systems, a different control strategy is used in this work, which offers several advantages over the existent filtering solutions as it will be discussed in the next sections. The benefits of the developed solution are:

1. Simple and low-cost hardware implementation,
2. Notable reduction of the switching frequency and reduced torque ripples,
3. The high impedance state of inverter legs is not used, which allows using cost-effective driver circuits with internally-set dead time.

The proposed method is detailed through the next sections of the paper. The first section presents description and mathematical modelling of the electrical drive system including the filter and the BLDC motor. The advantages of the proposed configuration are discussed and analysed. Section 2 presents the conventional trapezoidal control of the BLDC motor based on a simple PI-controller and a high-frequency PWM technique. The improved control strategy based on an LC filter is also developed in this section. Finally, simulation results are analyzed in Section 4 and performances are compared with the conventional trapezoidal control.

www.czasopisma.pan.pl PAN POLSKA AKADEMIA NAUK www.journals.pan.pl



## 2. System description and modeling

The power chain of the investigated system based on LC filtering is illustrated by Fig. 1. The BLDC motor is connected to a battery-powered six-switch inverter. $E$ is the battery voltage. An LC filter is connected between the inverter and the motor to remove the high-frequency components of the output current.

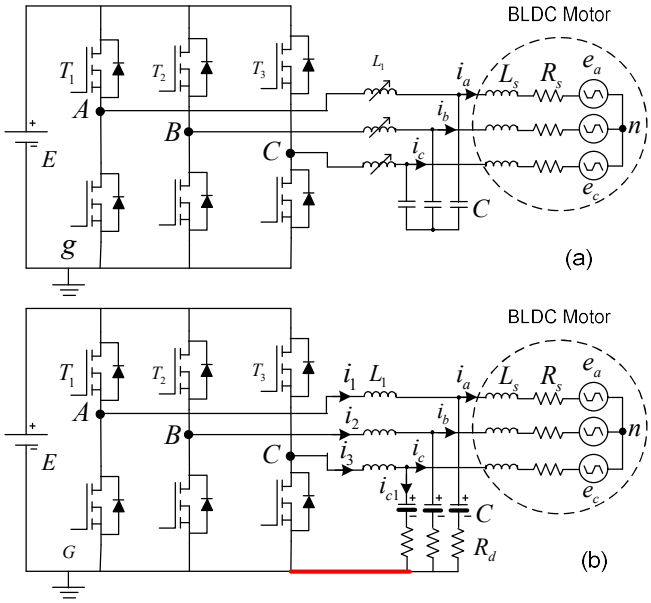


Fig. 1. Topology of the drive system with LC filter: (a) topology with servo-controlled inductors [13]; (b) proposed topology with polarized capacitors

### 2.1. Characteristics of the proposed configuration

In the solution presented in [13], the LC filter is built up through servo-controlled inductors along with fixed capacitor elements. The value of the inductors is adjusted according to the rotor speed. Actually, the filter topology is identified to a third order LCL filter, if the inductance of the stator windings $L_s$ is considered. The size of the filter elements defines the resonance frequency $\omega_{\text{res}}$. The expression of $\omega_{\text{res}}$ is given by [14]:

$$\omega_{\text{res}} = \sqrt{\frac{L_1 + L_s}{L_1 L_s C}}. \tag{1}$$

For efficient filtering performances, the resonance frequency should be selected below the desired switching frequency $\omega_{sw}$. As it can be deduced from Eq. (1), lower resonance frequencies are obtained by increasing the filter inductance $L_1$ or the filter capacitor value $C$. According to the configuration of Fig. 1(a), the sum of currents flowing through the filter capacitors is equal to zero: $i_{c1} + i_{c2} + i_{c3} = 0$. Thus, voltage oscillations across the capacitive elements satisfy the following relation:

$$C\frac{\mathrm{d}\left(v_{c1} + v_{c2} + v_{c3}\right)}{\mathrm{d}t} = 0. \tag{2}$$

www.czasopisma.pan.pl PAN POLSKA AKADEMIA NAUK www.journals.pan.pl



From relation (2), it is obvious that capacitors may operate with negative voltage across their terminals and therefore, it is necessary to use non-polarized ceramic or film capacitors. With this technology, capacitors can handle high AC voltages and capacitance values are typically between 1 nF and few μF. Capacitors with higher values may exist but they are potentially very expensive. Therefore, to reduce the resonance frequency, designers were constrained to use large inductances to achieve good filtering performances. For example, in [13], authors have proposed a variation range between 5 and 35 mH. However, magnetic elements are bulky, expensive and characterized by a limited saturation current. For these reasons, the configuration of Fig. 1(b) is proposed in this work to filter current harmonics through the stator phases. By connecting filter capacitors to the ground potential, it is possible to use polarized electrolytic capacitors, which allow obtaining large capacitance values at a low cost, and they have a larger equivalent serie resistor (ESR). The ESR can be considered as a low value damping resistor ($R_d$) used to attenuate the system response. With this configuration, it is possible to minimize the magnetic elements and to obtain low resonance frequencies through low-cost electrolytic capacitors. Unlike the conventional LC filtering, the topology of Fig. 1(b) can be considered as the combination of three reversible buck DC/DC converters which share the same input voltage $E$. Thus, an appropriate control strategy should be developed to impose constant DC voltages across the capacitors $C$ such that the current flowing through the motor windings are equal to the desired references. The control strategy of this system is based on active damping to attenuate voltage oscillations and it is developed in Section 3.

### 2.2. System design and modelling

In BLDC motors, the magnetic field is provided by permanents magnets which create trapezoidal back-EMFs $e_{abc}$ through the three stator phases [15]. Using Kirchhoff laws, the motor operation is described by differential equations as follows:

$$\begin{cases} v_{AG} = L_1 \dfrac{\mathrm{d}i_1}{\mathrm{d}t} + v_{c1} + R_d i_{c1} \\ v_{BG} = L_1 \dfrac{\mathrm{d}i_2}{\mathrm{d}t} + v_{c2} + R_d i_{c2} \\ v_{CG} = L_1 \dfrac{\mathrm{d}i_3}{\mathrm{d}t} + v_{c3} + R_d i_{c3} \end{cases}, \tag{3}$$

$$\begin{cases} i_1 = i_{c1} + i_a \\ i_2 = i_{c2} + i_b \\ i_3 = i_{c3} + i_c \end{cases}. \tag{4}$$

$L_1$ and $C$ represent the filter inductance and capacitance. In addition, system topology allows writing the following relations:

$$\begin{cases} v_{c1} + R_d i_{c1} = L_s \dfrac{\mathrm{d}i_a}{\mathrm{d}t} + R_s i_a + e_{an} + e_{nG} \\ v_{c2} + R_d i_{c2} = L_s \dfrac{\mathrm{d}i_b}{\mathrm{d}t} + R_s i_b + e_{bn} + e_{nG} \\ v_{c3} + R_d i_{c3} = L_s \dfrac{\mathrm{d}i_c}{\mathrm{d}t} + R_s i_c + e_{cn} + e_{nG} \end{cases}. \tag{5}$$

$R_s$ stands for the resistance of the stator windings and $L_s$ is the equivalent cyclic inductance. $e_{ng}$ stands for the voltage between the neutral point connection and the ground potential $G$. Furthermore, the high-side MOSFETs of the inverter are controlled with the PWM signals referred to as $T_1$, $T_2$ and $T_3$. If, the duty cycles of these signals are noted $\alpha_1$, $\alpha_2$ and $\alpha_3$; the average values of the phase-to-ground voltages are expressed by

$$v_{(A,B,C)G} = \alpha_{(1,2,3)} E. \tag{6}$$

The above equation can be used to derive the transfer function of the filter. For example, for phase $A$, Eqs. (3), (4) and (5) give:

$$v_{AG} = (L_1 + L_s)\frac{\mathrm{d}i_a}{\mathrm{d}t} + R_s i_a + L_1 C\frac{\mathrm{d}v_{c1}}{\mathrm{d}t} + e_{aG}, \tag{7}$$

$$v_{c1} + R_d C\frac{\mathrm{d}v_{c1}}{\mathrm{d}t} = L_s\frac{\mathrm{d}i_a}{\mathrm{d}t} + R_s i_a + e_{aG}. \tag{8}$$

By inserting Eq. (7) into (6), the following transfer functions are obtained:

$$G_1(s) = \frac{i_a}{v_{AG}} = \frac{R_d C s + 1}{D(s)}, \tag{9}$$

$$G_2(s) = \frac{i_a}{e_{aG}} = \frac{L_1 C s^2 + R_d C s + 1}{D(s)}, \tag{10}$$

with:

$$D(s) = L_1 C L_s s^3 + (R_d C\,(L_1 + L_s) + L_1 C R_s)\,s^2 + ((L_1 + L_s) + R_s R_d C)\,s + R_s.$$

Thus, the system configuration leads to third order transfer functions. $G_1(s)$ represents the influence of the input voltage on the current $i_a$ while $G_2(s)$ stands for the effect of the back EMF on this current. The switching frequency $f_{sw}$ of power transistors is chosen equal to 10 kHz. The resonance frequency should be in the interval between the rated frequency of the motor and the switching frequency. For efficient filtering performances, this frequency is chosen equal to 4 kHz. This value is achieved by maximizing the capacitor value $C$ and minimizing the inductance $L_1$. Taking standard polarized capacitors of 100 μF, the value of the filter inductance is calculated through relation (1), and it is equal to 0.47 mH. $R_d$ is equal to 0.15 Ω. With this choice of filter elements, the Bode diagram of the system $G_1(s)$ is plotted in Fig. 2. The obtained frequency response shows that the amplification is effectively reduced at the resonance frequency due to the insertion of the damping resistors. Also, it is observed that the LC filter improves the filtering performances at the switching frequency by 12 dB compared with the case where only an inductive filter with the same inductance value $L_1$ is used.

Finally, the parameters of the drive system with the configuration of Fig. 1(b) are summarized in Table 1.

www.czasopisma.pan.pl PAN POLSKA AKADEMIA NAUK www.journals.pan.pl



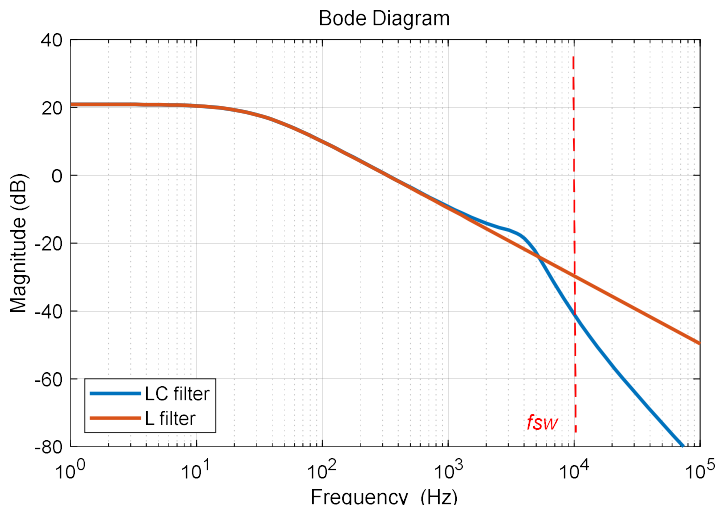


Fig. 2. Bode diagram of the system $G_1(s)$

Table 1. Parameters of the drive system

| Parameter | Symbol | Value | Unit |
|---|---|---|---|
| Rated power | $P_r$ | 90 | W |
| Rated current | $I_s$ | 10 | A |
| Pole pairs | $p$ | 7 | – |
| Voltage constant | $K_v$ | 1 | V/krpm |
| Stator resistance | $R_s$ | 0.09 | Ω |
| Synchronous inductance | $L_s$ | 0.015 | mH |
| DC bus voltage | $E$ | 12 | V |
| Filter inductance | $L_1$ | 0.47 | mH |
| Filter capacitance | $C$ | 100 | μF |
| Switching frequency | $f_{sw}$ | 10 | kHz |
| Sampling period | $T_s$ | 100 | μs |

## 3. Conventional trapezoidal control

Figure 3 presents the main elements of the conventional control strategy. The ideal waveforms of currents according to this control technique are shown in Fig. 4. A *Proportional-Integral* controller is used to impose quasi-square currents through the stator windings. The maximum value of $\{i_a, i_b, i_c\}$ is used as input for the current controller. To impose a constant torque, the

PWM duty cycle $\alpha(t)$ is kept constant until commutation information is delivered by the position sensors. At this instant, the switching logic changes the gate signals delivered to each power MOSFET. Gate signals are represented in Fig. 5.

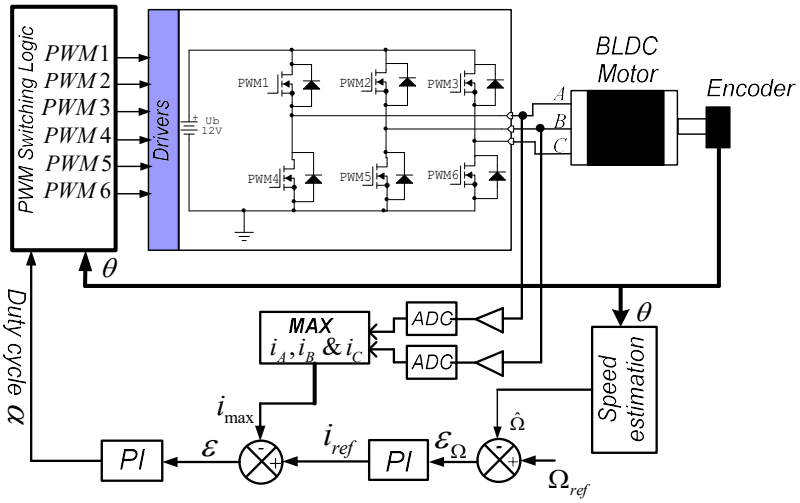


Fig. 3. BLDC-based electrical drive system with trapezoidal control strategy [16]

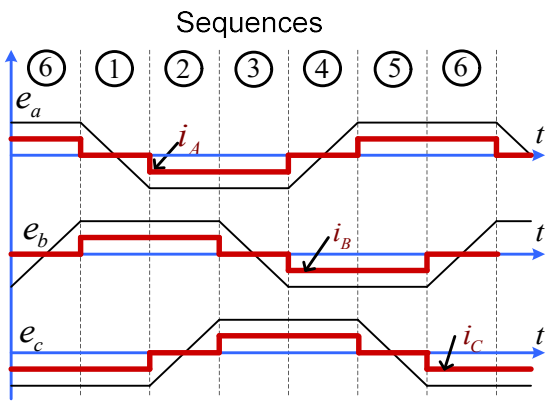


Fig. 4. Timing diagram of ideal currents and back-EMFs in BLDC motors according to the trapezoidal control

The maximum torque is obtained when the stator magnetic field is leading the rotor field by 90 electrical degree. Considering that only two stator phases are energized at each instant, it is obvious that the stator field can take only six directions according to the six possible current direction. Thus, to obtain maximum torque, the appropriate current direction is active when the rotor is phase-lagging the static alignment by 120°. When the rotor reaches 60° with respect to the alignment, the next current direction is activated and the process repeats. In this way, the phase shift between the stator field and the rotor field undergoes a 30° oscillation with respect to the ideal value of 90°.

www.czasopisma.pan.pl PAN POLSKA AKADEMIA NAUK www.journals.pan.pl



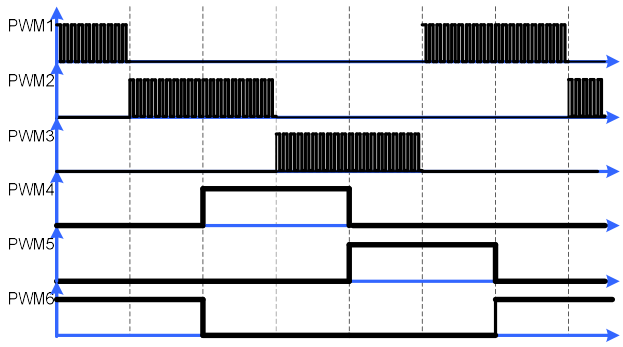


Fig. 5. Gate-to-source signals for power MOSFETs when conventional trapezoidal control is used

## 4. Proposed control strategy of the BLDC motor

The block diagram of the control strategy is depicted in Fig. 6. As it can be observed, the control signals of the power MOSFETs, $T_1$, $T_2$ and $T_3$ are synthesized only through three separate single-phase current controllers. Current references, $i_a^*$, $i_b^*$ and $i_c^*$, are generated in each commutation sequences based on the detected rotor position $\theta$. The design of this control strategy is performed in the following sections.

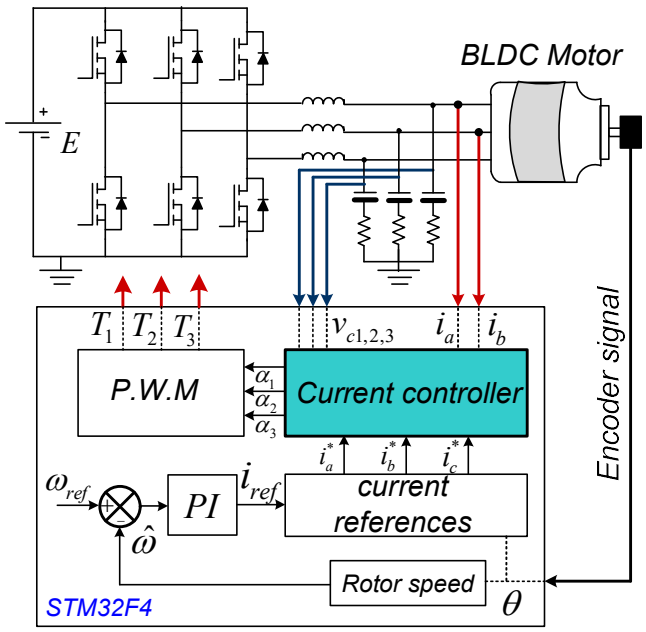


Fig. 6. Proposed control strategy of the BLDC motor with LC filtering

### 4.1. Design of current controllers with active damping

The ultimate objective of the proposed controller is to impose appropriate voltages across the filter capacitors $C$ such that winding currents are equal to the desired references. In this way, the motor fed with constant DC voltages will operate with a reduced level of currents and torque ripples. However, during phase commutations, the resonance phenomena lead to an oscillating transient response of the system. Even though the system includes passive damping components ($R_d$ and $R_s$), a single-loop feedback controller is not sufficient to mitigate system oscillations due to the LCL resonance [17]. Therefore, an active damping scheme is adopted in this work to control the phase currents. Active damping may be performed by measuring currents or voltages across the filter capacitors. Nevertheless, in this application, it is reasonable to use capacitor voltages since they are characterized by a low level and it is possible to detect them through low cost circuitry. Figure 7 shows the adopted dual-loop controller to attenuate resonance oscillations. Active damping is used for the capacitor voltage $v_{c1}$. The damping transfer function is noted $K(s)$ [18]. The same configuration is used for controlling currents in phases $B$ and $C$.

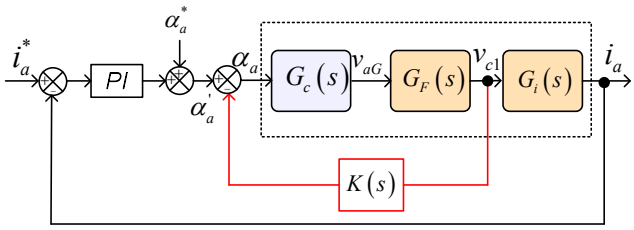


Fig. 7. Single-phase controller with active damping based on capacitor voltages

$\alpha_a$ is the generated duty cycle to control the high-side transistor and $G_c(s)$ represents the converter transfer function. For simplicity, the converter is represented by a simple gain equal to the DC link voltage $E$. The effect of the damping resistor is not considered for the controller design due to its low value.$G_F(s)$ stands for the filter transfer function and $G_i(s)$ is the transfer function which relates the phase current to the capacitor voltage. Their expressions are given by:

$$G_F(s) = \frac{v_{c1}}{v_{AG}}(s) = \frac{1}{L_1 C}\frac{}{s^2 + \omega_{\text{res}}^2}, \tag{11}$$

$$G_i(s) = \frac{i_a}{v_{c1}}(s) = \frac{1}{L_s s}. \tag{12}$$

$K(s)$ provides active damping to prevent voltage oscillations. With the feedback $K(s)$, the transfer function of the inner loop is written as:

$$G_{F_AD}(s) = \frac{G_c(s)G_F(s)}{1 + K(s)G_c(s)G_F(s)}. \tag{13}$$

The system response is analysed with various feedback types in order to achieve the best stabilization performances. The feedback types are the proportional, derivative and integral actions. The global transfer function with these feedbacks are given:

www.czasopisma.pan.pl PAN POLSKA AKADEMIA NAUK www.journals.pan.pl



– Proportional: $K(s) = k_a$,

$$G_{F_AD}(s) = \frac{\frac{E}{L_1 C}}{s^2 + \left(\omega_{\text{res}}^2 + k_a \frac{E}{L_1 C}\right)}, \tag{14}$$

– Derivative: $K(s) = k_a s$,

$$G_{F_AD}(s) = \frac{\dfrac{E}{L_1 C}}{s^2 + \dfrac{k_a E}{L_1 C} s + \omega_{\text{res}}^2}, \tag{15}$$

– Integral: $K(s) = \dfrac{k_a}{s}$,

$$G_{F_AD}(s) = \frac{Es}{L_1 C s^3 + L_1 C \omega_{\text{res}}^2 s + k_a E}. \tag{16}$$

Equation (14) shows that the proportional feedback leads to a second order transfer function with two imaginary poles and the natural frequency increases when $k_a$ is increased. Therefore, the proportional action cannot prevent voltage oscillations. When using the integral action, the Routh-Hurwitz criterion applied to Eq. (16) allows inferring that the system becomes unstable. Finally, with the derivative feedback the system is identified to a second order transfer function and it is possible to set the damping ratio through the gain $k_a$. Also, the natural frequency remains constant and equal to $\omega_{\text{res}}$ as $k_a$ increases. Thus, derivative feedback is to achieve efficient damping performances. However, since a digital computer is used for the implementation of the control algorithm, the value of the feedback gain will be set using the discrete-time representation. As first consideration, the sampling frequency is chosen such that it is 6 to 24 times higher than the system cut-off frequency in closed loop [19]. The calculation of the derivative terms of the feedback voltage is achieved through a backward differentiation scheme. In addition, it is assumed that the PWM block of the power converter introduces a time delay equal to the sampling frequency [18–20]. Thus, using the *z-transformation*, the inner loop controller can be represented in the $z$−domain by the bloc diagram of Fig. 8.

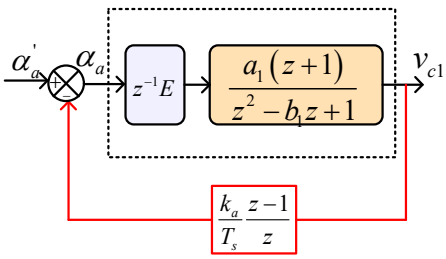


Fig. 8. Representation of the inner loop in the $z$-domain

www.czasopisma.pan.pl PAN POLSKA AKADEMIA NAUK www.journals.pan.pl



In Fig. 8, $a_1 = 0.05779$, $b_1 = 1.737$. The MATLAB command 'c2d' was used to calculate these coefficients based on the "zero order hold" method. The transfer function of the inner loop in the $z-$domain is written as:

$$H_F(z) = \frac{a_1 E z\,(z+1)}{z^4 + b_1 z^3 + \left(1 + \dfrac{k_a}{T_s} a_1 E\right) z^2 - \dfrac{k_a}{T_s} a_1 E}. \tag{17}$$

Figure 9 shows the pole-zero map of the discrete transfer function when the gain $k_a$ varies from 0 to 3e-5. As it can be observed, the open loop system includes two poles located on the unity circle which leads to an oscillatory behaviour of the capacitor voltages. Initially, when $k_a$ is increased, system poles are shifted towards the stability region which results in a damped response of the system. However, when $k_a$ exceeds a certain value, the trajectory deviates and the pole locations move outside of the unity circle. Therefore, the gain $k_a$ is chosen at the middle of the stability interval to obtain good resonance damping and to ensure the stability of the system.

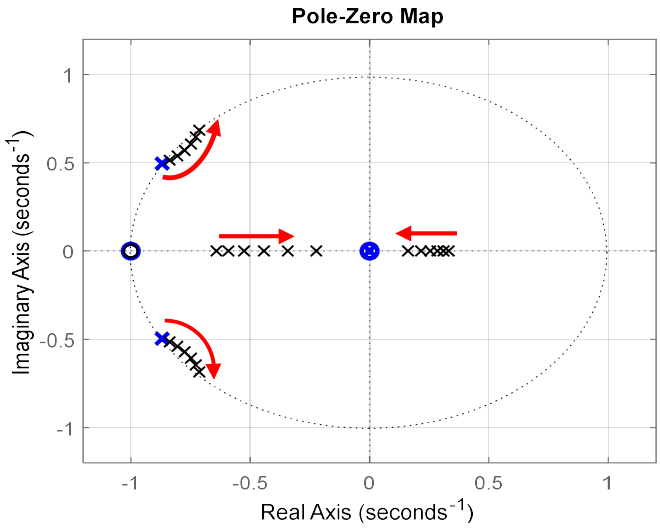


Fig. 9. Pole-zero map of the inner loop for different values of the derivative gain $k_a$: blue – without feedforward; black – with feedforward

Furthermore, the outer loop is used to control phase currents through PI controllers. The parameters of these controllers are tuned considering the block diagram of Fig. 7 and taking into account the value of the derivative feedforward identified through the above analysis. Considering the system representation in Fig. 7, the open loop transfer function is written as:

$$G_{OL}(s) = \frac{k_i \left(1 + \dfrac{k_p}{k_i} s\right) \dfrac{E}{L_1 C L_s}}{s^2 \left(s^2 + \dfrac{k_a E}{L_1 C} s + \omega_r^2\right)}. \tag{18}$$

www.czasopisma.pan.pl PAN POLSKA AKADEMIA NAUK www.journals.pan.pl



The system of Fig. 7 is stable in normal operation if the phase margin of the open loop transfer function $G_{OL}(s)$ remains positive [21]. That is, the phase of $G_{OL}(s)$ at the crossover frequency $\omega_{co}$ (0 dB gain) should remain positive. The phase margin is defined as:

$$PM = 180^\circ + \phi\left(\omega = \omega_{co}\right). \tag{19}$$

The parameters of the PI controller are designed such that a typical phase margin of 60° is obtained. The frequency response of $G_{OL}(s)$ is plotted in Fig. 10.

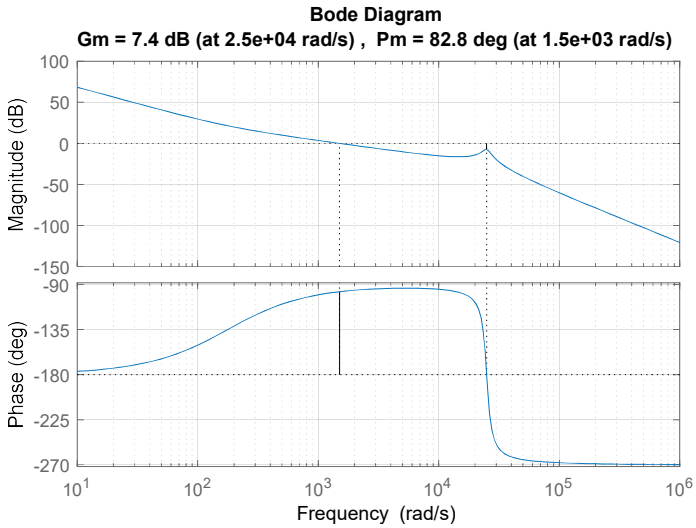


Fig. 10. Bode plot of the open loop system with PI controller

### 4.2. Generation of voltage current references

The key point in the proposed control method is to supply the terminals of the BLDC motors with constant DC voltages in order to overcome the issue of low inductance value. In this case, currents flowing through the stator windings are the results of voltage differences between stator phases. In steady state, the relationship between the input voltages and the phase currents can be identified through Eqs. (3) and (5). The steady-state relationships are identified using the averaging operator defined as [22]:

$$\overline{x}(t) = \frac{1}{T_s}\int_{t}^{t+T_s} x\left(\tau\right)\mathrm{d}\tau, \tag{20}$$

where $x(t)$ is a variable and the overbar denotes its average. By applying the averaging operator over Eqs. (3) and (5), the following results are obtained:

$$\begin{cases} \alpha_a E = \overline{v}_{c1} \\ \alpha_b E = \overline{v}_{c1} \\ \alpha_c E = \overline{v}_{c2} \end{cases}, \tag{21}$$

$$\begin{cases} \overline{v}_{c1} = R_s \overline{i}_a + \overline{e}_{aG} \\ \overline{v}_{c2} = R_s \overline{i}_b + \overline{e}_{bG} \\ \overline{v}_{c3} = R_s \overline{i}_c + \overline{e}_{cG} \end{cases}. \tag{22}$$

The coupling between phase currents is expressed by the relation $i_a + i_b + i_c = 0$. Also, the sum of the back-EMFs can be assumed equal to 0 ($e_a + e_b + e_c = 0$). Considering relations (22) and (21), it is possible to show that:

$$\begin{pmatrix} \overline{i}_a \\ \overline{i}_b \\ \overline{i}_c \end{pmatrix} = \frac{E}{3R_s} \begin{pmatrix} 2 & -1 & -1 \\ -1 & 2 & -1 \\ -1 & 2 & -1 \end{pmatrix} \begin{pmatrix} \alpha_a \\ \alpha_b \\ \alpha_c \end{pmatrix} - \begin{pmatrix} \overline{e}_a \\ \overline{e}_b \\ \overline{e}_c \end{pmatrix}. \tag{23}$$

By considering back-EMFs as disturbance signals, Eq. (23) can express the relation between the phase currents and the duty cycles controlling the inverter output voltages. As it can be observed, currents and duty cycles are linked by a singular matrix which indicates that for a given combination of reference currents $i_a^*$, $i_b^*$, and $i_c^*$, there exist several combinations of duty cycles ($\alpha_a^*$, $\alpha_b^*$ and $\alpha_c^*$) which allow generating the desired references. It is important to impose reference duty cycles to avoid the saturation of the PWM block during transient regimes, that is, when the operation point becomes close to the extremums of the generated voltage ($\alpha_i^* = 0$, or $\alpha_i^* = 1$). Therefore, duty cycles are selected such that the capacitor voltages are kept as close as possible to the half of the DC link. For example, during sequence (1), current references are shown in Fig. 4 and they are equal to $i_a^* = 0$, $i_b^* = i_{\text{ref}}$ and $i_c^* = -i_{\text{ref}}$. To impose these references, the steady-state duty cycles are calculated as:

$$\begin{cases} \alpha_a^* = 0.5 \\ \alpha_b^* = 0.5 + d \\ \alpha_c^* = 0.5 - d \end{cases}, \tag{24}$$

with $d = \left(\dfrac{3R_s}{E}\right) i_{\text{ref}}$.

Finally, current references are generated based on the rotor position and the output of the speed controller $i_{\text{ref}}$. The ideal current waveforms in each commutation sequence are represented in Fig. 4. Table 2 gives the values of current and duty cycle references according to the rotor position $\theta$.

Table 2. Generated current and duty cycle references according to the rotor position

| **Sequence** | **1** | **2** | **3** | **4** | **5** | **6** |
|---|---|---|---|---|---|---|
| $\theta$ | 0–60° | 60–120° | 120–180° | 180–240° | 240–300° | 300–360° |
| $i_a^*$ | 0 | $-i_{\text{ref}}$ | $-i_{\text{ref}}$ | 0 | $i_{\text{ref}}$ | $i_{\text{ref}}$ |
| $i_b^*$ | $i_{\text{ref}}$ | $i_{\text{ref}}$ | 0 | $-i_{\text{ref}}$ | $-i_{\text{ref}}$ | 0 |
| $i_c^*$ | $-i_{\text{ref}}$ | 0 | $i_{\text{ref}}$ | $i_{\text{ref}}$ | 0 | $-i_{\text{ref}}$ |
| $\alpha_a^*$ | 0.5 | $0.5 - d$ | $0.5 - d$ | 0.5 | $0.5 + d$ | $0.5 + d$ |
| $\alpha_b^*$ | $0.5 + d$ | $0.5 + d$ | 0.5 | $0.5 - d$ | $0.5 - d$ | 0.5 |
| $\alpha_c^*$ | $0.5 - d$ | 0.5 | $0.5 + d$ | $0.5 + d$ | 0.5 | $0.5 - d$ |

www.czasopisma.pan.pl PAN POLSKA AKADEMIA NAUK www.journals.pan.pl



## 5. Analysis of performances

This section presents the motor operation with the developed control strategy. The obtained results are compared with the conventional trapezoidal control which uses the OFF state for both the high-side and the low-side transistors in the same leg in order to impose a zero current through the open phase.

### 5.1. Operation with the LC filter

The behaviour of the BLDC motor during the starting-up is shown in Fig. 11. According to the desired acceleration ramp, the rotor speed should increase from zero to reach 500 rpm within a time interval of 0.5 s (Fig. 11(a)). During the acceleration time, the oscillations of the electromagnetic torque are limited and they do not exceed 10% of the average value as shown in Fig. 11(b). Figure 11(c) gives the current waveforms in the three phases. As it can be observed, current ripples at the switching frequency are totally removed by the LC filter. Also, during current commutations between two phases, the current in the third phase remains stable and equal to the reference value. This characteristic explains the stable torque behaviour during commutations. Figure 11(d) shows capacitor voltages. Voltages remain stable after each commutation due to the active damping loop. The currents flowing through these capacitors are represented in Fig. 11(e). These currents oscillate at the switching frequency and the peak-to-peak value do not exceed 1 A.

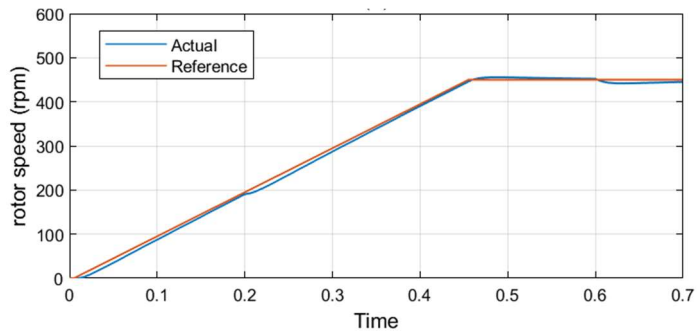


(a)

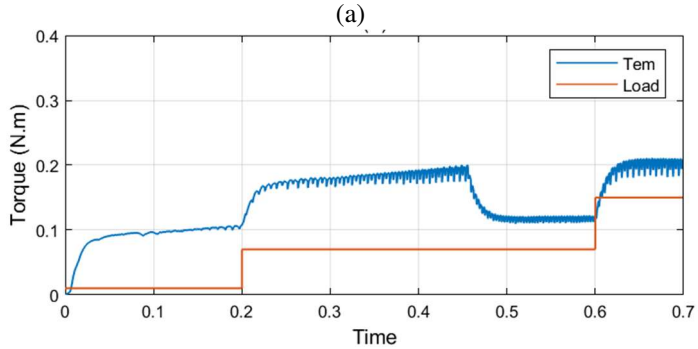


(b)

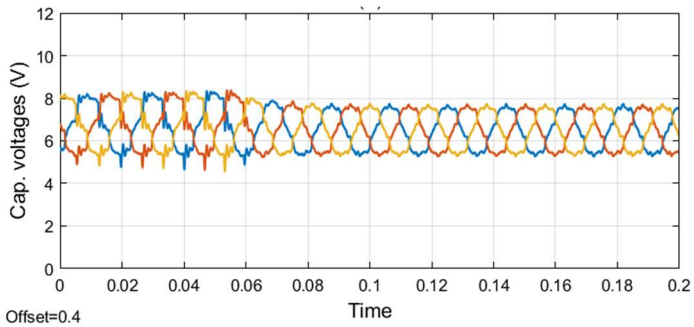


(d)

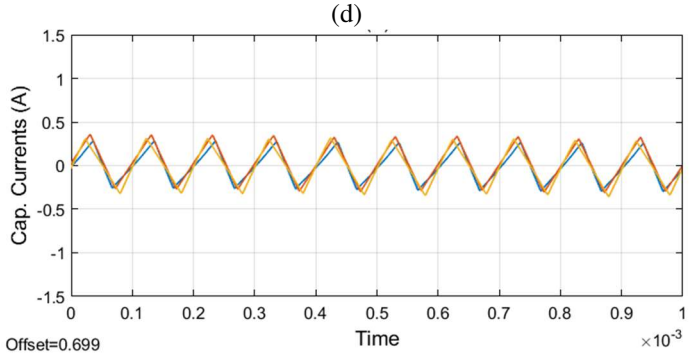


(e)

Fig. 11. Operation of the BLDC motor with LC filtering and active damping: (a) rotor speed; (b) torque; (c) phase currents; (f) capacitors voltages; (e) currents in the capacitive elements

### 5.2. Operation with the conventional trapezoidal control

To illustrate the advantages of the proposed technique, this section analyses the behaviour of the BLDC motor when the conventional trapezoidal control is applied. This method is widely used on the industrial scale and it was detailed in Section 2. Figure 12 shows the obtained results when the switching frequency of power transistors is equal to 100kHz. Figure 12(a) shows that the rotor speed follows the acceleration ramp and the error becomes equal to zero in steady state. However, phase currents present a highly oscillating component that influences the stability of the developed

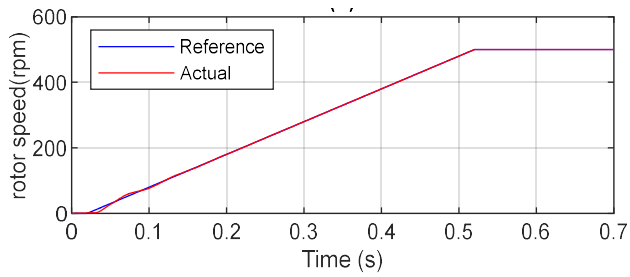


(a)

www.czasopisma.pan.pl PAN POLSKA AKADEMIA NAUK www.journals.pan.pl



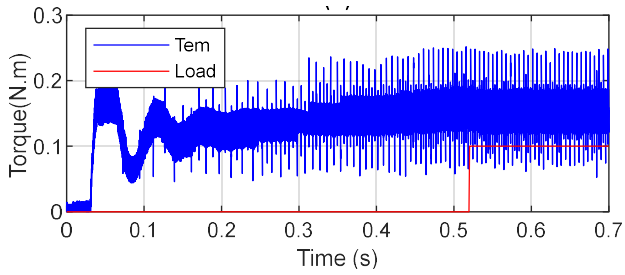


(b)

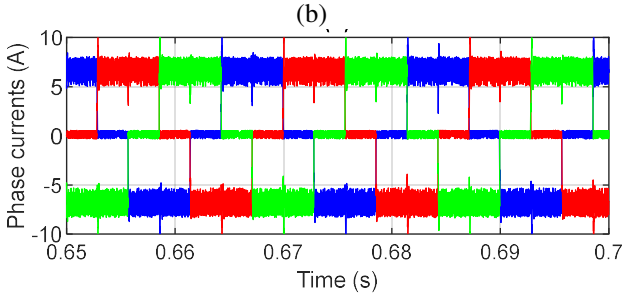


(c)

Fig. 12. Control of the BLDC motor with the conventional trapezoidal control ($f_{sw}$ = 100 kHz)

torque. Although, the increase of the switching frequency by a ratio of ten, torque ripples remain considerable, which results in higher audible noise, higher switching losses in power transistors, vibration and Electromagnetic Interferences (EMI).

Furthermore, the motor operation with trapezoidal control was tested when a simple inductive filter is used between the inverter and the stator windings. In this configuration, the value of the filter inductance and the switching frequency are chosen the same as in Table 1, that is, the same values used in the configuration with the LC filter. Figure 13(a) shows that the rotor speed follows the imposed acceleration ramp. In Fig. 13(b), it is observed that the inductive filter effectively attenuates torque ripples due to the switching frequency. When the rotor speed increases, the electromagnetic torque is subject to perturbations of considerable importance. Indeed, the inserted inductances increase the rise and fall times during commutations, which generates torque oscillations as shown in Fig. 13(b) and Fig. 13(c). However, with the method based on LC filtering and active damping, torque ripples are minimized during low or high speeds which illustrates the benefits of this method.

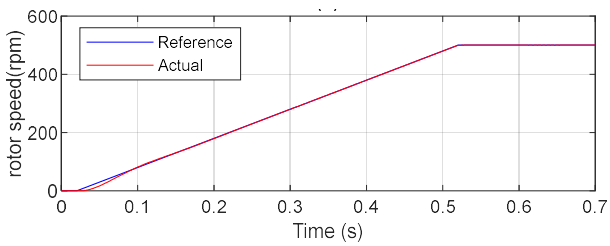


(a)

www.czasopisma.pan.pl PAN POLSKA AKADEMIA NAUK www.journals.pan.pl



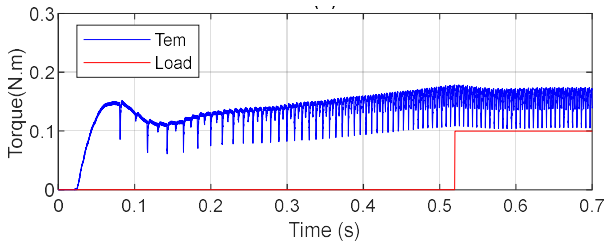


(b)

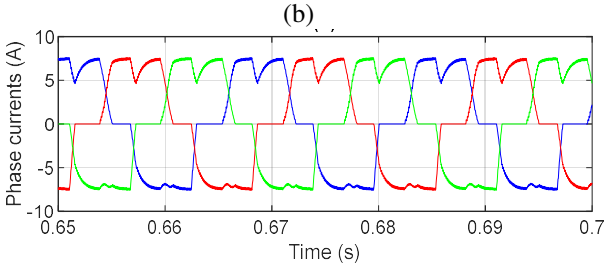


(c)

Fig. 13. Operation of the BLDC motor with an inductive filter ($L_1$ = 0.47 mH, $f_{sw}$=100 kHz)

## 6. Conclusions

In this paper, an improved method to implement trapezoidal current control of BLDC motors was proposed. This method allows reducing torque ripples using a single-stage conversion system without increasing the switching frequency of the inverter. It is also possible to reduce the generated EMI without over-complicating the overall control strategy. Also, the proposed method represents an additional advantage of generating only three gate signals of the high-side transistors. The low-side transistors are controlled with complementary signals which can be generated by low-cost drivers. This configuration is not possible with the conventional control method, where it is mandatory to provide a separate control signal for each power switch, which will increase the cost and complexity of the design. These improved performances require three additional voltage sensors to measure capacitor voltages. It is possible to use optical isolation amplifiers, which offer precision voltage sensing at a reasonable cost. Finally, a BLDC motor with integrated hall sensors can be used for position and speed estimation. In this case, the encoder can be removed to further reduce the implementation cost of the proposed system.

**Acknowledgements**

This work was supported by the Tunisian Ministry of High Education and Scientific Research under the PEJC project: 21PEJC D6P1.

**References**

[1] Mousmi A., Abbou A., El Houm Y., *Trapezoidal control of Brushless DC motor based on DSP F28335*, International Conference on Wireless Technologies, Embedded and Intelligent Systems, Fez, Morocco (2017), DOI: 10.1109/WITS.2017.7934602.

[2] Mohanraj D., Aruldavid R., Verma R. *et al.*, *A Review of BLDC Motor: State of Art, Advanced Control Techniques, and Applications*, IEEE Access, vol. 10, pp. 54833–54869 (2022), DOI: 10.1109/ACCESS.2022.3175011.

[3] Seo M.K., Lee T.Y., Ko Y.Y., Kim Y.J., Jung S.Y., *Irreversible demagnetization analysis with respect to winding connection and current ripple in brushless DC motor*, IEEE Transaction on Applied Superconductivity, vol. 28, no. 3, pp. 1–4 (2018), DOI: 10.1109/TASC.2018.2792449.

[4] Krishnan R., *Permanent Magnet Synchronous Brushless DC Motor Drives*, CRC Press (2010).

[5] Fang J., Zhou X., Liu G., *Instantaneous Torque Control of Small Inductance Brushless DC Motor*, IEEE Transaction on Power Electronics, vol. 27, no. 12, pp. 4952–4964 (2012), DOI: 10.1109/TPEL.2012.2193420.

[6] Li W., Fang J., Li H., Tang J., *Position Sensorless Control without Phase Shifter for High-Speed BLDC Motors with Low Inductance and Non-ideal Back EMF*, IEEE Transaction on Power Electronics, vol. 31, no. 2, pp. 1354–1366 (2016), DOI: 10.1109/TPEL.2015.2413593.

[7] Feng J., Liu K., Wang Q., *Scheme based on buck converter with three phase H-bridge combinations for high speed BLDC motors in aerospace applications*, IET Electric Power Applications, vol. 12, no. 3, pp. 405–414 (2018), DOI: 10.1049/iet-epa.2017.0615.

[8] Li H., Li W., Ren H., *Fault-Tolerant Inverter for High-Speed Low-Inductance BLDC Drives in Aerospace Applications*, IEEE Transaction on Power Electronics, vol. 32, no. 3, pp. 2452–2463 (2017), DOI: 10.1109/TPEL.2016.2569611.

[9] Feng Z., Ramesh RR., Ebrahimi S. *et al.*, *Control Strategy for Torque Ripple Reduction in Brushless DC Motors with 180-Degree Commutation*, IEEE 6th Global Power, Energy and Communication Conference, Budapest, Hungary (2024), DOI: 10.1109/GPECOM61896. 2024.10582640.

[10] Lee J., Lim G.C., Ha J.I., *Pulse Width Modulation Methods for Minimizing Commutation Torque Ripples in Low Inductance Brushless DC Motor Drives*, IEEE Transactions on Industrial Electronics, vol 70, no. 5, pp. 4537–4547 (2023), DOI: 10.1109/TIE.2022.3189104.

[11] Valle R.L., De Almeida P.M., Fogli G.A., Ferreira A.A., BarbosabP.G., *Simple and Effective Digital Control of a Variable-Speed Low Inductance BLDC Motor Drive*, IEEE Access, vol. 8, pp. 13240–13250 (2020), DOI: 10.1109/ACCESS.2020.2966437.

[12] Pandey M.K., Tripathi A., Dwivedi B., *A technique to minimize the effect of current harmonics in a brushless dc motor drive*, IEEE 10th Conference on Industrial Electronics and Applications, Auckland, New Zealand, pp. 9–21 (2015), DOI: 10.1109/ICIEA.2015.7334199.

[13] Chaudhari P.S., Patil S.L., *Reduction in Harmonics of BLDC Motor Drive Using Controlled LC Filter*, Electric Power Components and Systems, vol. 46, pp. 1686–1703 (2018), DOI: 10.1080/15325008.2018.1511007.

[14] Channegowda P., John V., *Filter Optimization for Grid Interactive Voltage Source Inverters*, IEEE Transactions on Industrial Electronics, vol. 57, no. 12, pp. 4106–4114 (2010), DOI: 10.1109/TIE.2010.2042421.

[15] Drozdowski P., *Modelling of BLDCM with a double 3-phase stator winding and back EMF harmonics*, Archives of Electrical Engineering, vol. 64, no. 1, pp. 53–66 (2015), DOI: 10.1515/aee-2015-0006.

[16] Baszynski M., *Torque ripple reduction in BLDC motor based on a PWM technique for open-end winding*, Archives of Electrical Engineering, vol. 70, no. 1, pp. 5–23 (2021), DOI: 10.24425/aee.2021.136049.

[17] Dannehl J., Fuchs F.W., Hansen S., Thogersen P.B., *Investigation of active damping approaches for PI-based current control of grid-connected pulse width modulation converters with LCL filters*, IEEE Transaction on Industry Applications, vol. 46, no. 4, pp. 1509–1517 (2010), DOI: 10.1109/TIA.2010.2049974.

[18] Parker S.G., McGrath B.P., Holmes D.G., *Regions of Active Damping Control for LCL Filters*, IEEE Transaction on Industry Applications, vol. 50, no. 1, pp. 424–432 (2014), DOI: 10.1109/ECCE.2012.6342412.

www.czasopisma.pan.pl PAN POLSKA AKADEMIA NAUK www.journals.pan.pl



[19] Landau I.D., Zito G., *Digital control systems*, Springer-Verlag (2006).
[20] Buso S., Mattavelli P., *Digital Control in Power Electronics*, Morgan and Claypool (2006).
[21] Levine W.S., *The Control Handbook*, CRC press, IEEE press (2000).
[22] Yazdani A., Irevani R., *Voltage Source Converters in Power Systems*, John Wiley & Sons (2010).